Relationship Between the Structure and Mechanical Properties of Polypropylene: Effects of the Molecular Weight and Shear-Induced Structure

Claudia Stern,[1] Achim Frick,[1] Günter Weickert[2]

[1]*Polymer Technology, Aalen University, Beethovenstrasse 1, 73430 Aalen, Germany*
[2]*Institute of Mechanics, Processes and Control-Twente, University of Twente, P.O. Box 217, 7500 AE Enschede, The Netherlands*

Received 15 November 2005; accepted 17 January 2006
DOI 10.1002/app.24156
Published online in Wiley InterScience (www.interscience.wiley.com).

ABSTRACT: A series of homopolymer polypropylenes (PPs), within a weight-average molecular weight (M_w) range of 100–1600 kg/mol, were manufactured as dumbbell microspecimens. The effects of the molecular weight and shear-induced crystallization on the mechanical properties and morphology were studied to gain a better understanding of the structure–property relationship. The results showed that the crystallinity decreased from 50 to 41% and the lamellar thickness increased as M_w increased. Tensile tests demonstrated that the stiffness and especially the tensile strength rose to extremely high values (Young's modulus = 2400 N/mm^2, stress at 30% strain = 120 N/mm^2). Furthermore, the strain hardening effect was strongly affected by the lamellar thickness and highly oriented superstructures. Dynamic mechanical analysis demonstrated that the mobility of the molecular chains depended on M_w and on the lamellar thickness. In addition, the viscoelastic properties of unannealed and annealed samples indicated further the existence of shish-kebab structures caused by shear-induced crystallization during injection molding. © 2006 Wiley Periodicals, Inc. J Appl Polym Sci 103: 519–533, 2007

Key words: mechanical properties; poly(propylene) (PP); shear; solid-state structure; structure-property relations

INTRODUCTION

The use of polymer products depends essentially on their stiffness, strength, deformability, and temperature and chemical resistance. These properties are mainly influenced by the molecular structure and processing conditions. For instance, the crystallinity and stiffness of a polymeric material is basically governed by the molecular structure (molecular weight and molecular weight distribution). Additionally, the acting flow and cooling conditions before and during the solidification of the molten polymer influence the crystallization and govern, therefore, the formation of the final structure.[1–10] For example, when high flow and cooling rates exist, oriented structures, such as shish-kebab or lamellar-row structures, are preferably formed. Nowadays, numerous studies have been carried out to analyze the influence of the flow on the morphology and properties of semicrystalline polymers[1–5,11,12]. Several techniques are in use to understand the effects of shear-induced crystallization. Thereby, the main idea is to study the origin of the nucleation and creation of structures *in situ* (during the crystallization of the molten polymer) caused by shearing. However, most of the experiments presented do not consider the influence of the shear-induced crystallization on the final properties. The reason is probably that most of the experiments are not performed on samples that can be analyzed in the solid state.

Nevertheless, the search for the relationship between the structures and properties has motivated extensive studies in the past. In particular, many analyses have been carried out to understand the dependence of the morphology on the deformation behavior of semicrystalline polymers.[13–21] Furthermore, there are many articles examining the influence of the processing conditions on the mechanical properties.[22–28]

However, the information available in the published literature is not sufficient for a complete understanding of the relationship between the molecular weight and final properties. The reason for this is the complexity of the structure–property relationship and the fact that mainly commercially available polymers are the subjects of scientific research. Because these materials usually include unknown additives (e.g., stabilizers, lubricants, and nucleation agents), a certain disadvantage exists, in that the research results are a complex mixture of unknown influencing factors that can act either synergistically or contrarily. Thus, the relationship between the structures and properties in the solid state can be defined successfully only when the main parameters are varied and studied systematically. For example, one of the main parameter is

Correspondence to: A. Frick (achim.frick@htw-aalen.de).

Journal of Applied Polymer Science, Vol. 103, 519–533 (2007)

TABLE I
Polymerization Conditions and Molecular Characteristics of the Synthesized PP Powders

Sample	Temperature (°C)	T_{max} (°C)	Pressure (bar)	H_2 (mol %)	M_w (kg/mol)	M_w/M_n	M_w/M_e
PP-L1600	70	70.6	35	0	1600[a]	NA	238
PP-L1120	70	71.9	52	0.02	1120	6.4	166
PP-L833	70	72.5	51	0.05	833	6.6	124
PP-L462	70	72.8	50	0.15	462	7.2	69
PP-L361	70	72.9	43	0.15	361	6.8	54
PP-L320	70	73.8	48	0.26	320	6.8	48
PP-L244	70	71.5	51	0.51	244	7.3	36
PP-L153	70	71.9	48	0.99	153	7.3	23
PP-L101	70	74.8	48	1.56	101[a]	NA	15

H_2, hydrogen content; M_e, entanglement molecular weight; M_n, number-average molecular weight; M_w, weight-average molecular weight; NA, not available; T_{max}, maximum temperature.
[a] Evaluated from rheological data.

the average molecular weight, which can be varied with different amounts of hydrogen during polymerization and with all other polymerization conditions kept constant.

This article studies the influence of the molecular weight and shear-induced structure on the mechanical properties of a series of injection-molded polypropylene (PP) specimens made from freshly synthesized PP. A major focus is the analysis of the mechanical response to static and dynamic deformation, which is critically important in determining the suitability of a material for a given application. In addition, the mechanical properties of injection-molded PP samples after annealing at 100 and 140°C are studied to analyze the effect of a possibly changed morphology and to better understand the structure–property relationship.

EXPERIMENTAL

The PP series studied in this article were prepared with a conventional Ziegler–Natta catalyst ($TiCl_4$/diester/$MgCl_2$ and triethyl aluminium/silane). All PP materials were synthesized with a novel liquid pool polymerization process. The polymerization was carried out in a 5-L stainless steel autoclave reactor completely filled with propylene under isothermal conditions.[29] Before the system was adjusted to the appropriate polymerization temperature of 70°C and pressure of about 60 bar, hydrogen was added as a chain-transfer agent to control the molecular weight. The polymerization reaction was terminated after approximately 60 min by the injection of methanol. The reactor was exhausted and cooled and afterwards was flushed several times with nitrogen to remove the last monomer. Finally, the powder was taken from the reactor and dried for 4 h in a vacuum oven at 50°C. Some main polymerization conditions and the specific properties of the synthesized PP powders are listed in Table I.

To these powders, 1% Irganox B215 (CIBA Specialty Chemicals, Grenzach, Germany) as a polymer stabilizer agent with an antioxidant and heat-stabilization effect was added to avoid the degradation of the polymer during the melting process.

The melting process was carried out under industrial-like conditions with an injection-molding machine (Allrounder S 220 150-30, Arburg, Lossburg, Germany). The machine was equipped with a newly developed screw and plasticizing unit, which was designed particularly for dosing microgranules or powders and for gentle processing of the polymer. The solidification process took place in a two-cavity mold with a temperature control system to control the mold temperature and keep it constant at a moderate temperature of 60°C during processing. With this mold, only a small amount of the polymer powder was required for manufacturing the dumbbell microspecimens, as illustrated in Figure 1. The main characteristics of the dumbbell microspecimens were a sample volume of 10 mm^3, a total length of 25 mm, and a cross-sectional area of 1.25 × 0.5 mm^2. The molding was performed at melt temperatures of 210 and 250°C and with a similar injection speed of 10 m/min; this depended on the specific injection pressure, which ranged from 500 to 1800 bars. In Table II, the processing conditions and the existing maximum shear rates of the samples are listed.

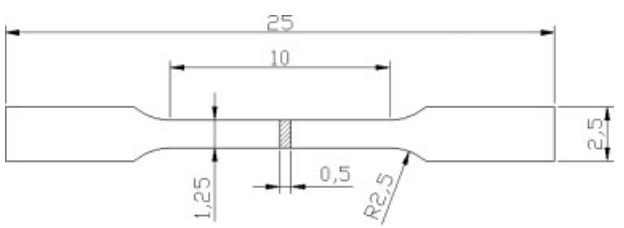

Figure 1 Dimensions of the dumbbell microspecimen.

TABLE II
Processing Conditions for Manufacturing Dumbbell Microspecimens and Existing Maximum Shear Rates

Sample	T_{melt} (°C)	T_{mold} (°C)	v_{inj} (m/min)	p_{inj} (bar)	p_h (bar)	t_{hp} (s)	t_c (s)	$\dot{\gamma}_{max}$ (s^{-1})
PP-L1600	250	60	10	1950	2000	4	15.4	7.0×10^5
PP-L1120	250	60	10	1400	1000	4	15.4	7.5×10^5
PP-L833	210	60	10	1600	1600	4	15.4	5.2×10^5
PP-L462	210	60	10	1540	1500	4	15.4	3.9×10^5
PP-L361	250	60	10	1000	1000	4	15.4	NA
PP-L320	210	60	10	520	500	4	15.4	3.0×10^5
PP-L244	250	60	10	900	1000	4	15.4	NA
PP-L153	250	60	10	1050	1000	4	15.4	NA
PP-L101	210	60	10	355	300	4	15.4	2.0×10^5

$\dot{\gamma}_{max}$, maximum shear rate; NA, not available; p_h, holding pressure; p_{inj}, injection pressure; t_c, cycle time; t_{hp}, holding pressure time; T_{melt}, melt temperature; T_{mold}, mold temperature; v_{inj}, injection speed.

Additionally, some samples were annealed in a convection oven for 1 h at 100 and 140°C to improve the perfection of the crystalline structure.

The differential scanning calorimetry (DSC) investigations were carried out in a temperature range of 30–280°C with a Mettler–Toledo differential scanning calorimeter 821^e (Scherzenback, Switzerland). A sample mass of 5.6 ± 0.1 mg of PP powder was placed in a 20-μL aluminum crucible and measured in a nitrogen atmosphere at a heating and cooling rate of 20 K/min.

The rheological investigations for analyzing the entanglement molecular weight were carried out in an oscillation mode with a Gemini 200 plate–plate rheometer from Bohlin Instruments (Herrenberg, Germany). At 200°C, a sinusoidal strain with constant amplitude of 1% was applied, and the angular frequency was logarithmically varied from 0.01 to 100 s^{-1}. The gap between both plates was 0.5 mm, and the measuring system was flushed with nitrogen to avoid any degradation of the polymer sample.

The uniaxial tensile tests were performed with a Gabo Qualimeter Eplexor 150 N dynamic mechanical analyzer (Ahlden, Germany) in a quasistatic mode. The dumbbell microspecimens were mounted between two clamping jaws at a distance of 15 mm with a contact force of 1 N. The measurements were performed at 25°C with a strain rate of 3×10^{-4} s^{-1}.

The viscoelastic properties were analyzed in a tensile mode with a Gabo Qualimeter Eplexor 150 N dynamic mechanical analyzer. The analyses were carried out in a temperature range from −50 to 150°C at a heating rate of 5 K/min. A contact force of 1 N was applied, and the oscillation amplitude of 0.2% strain, the static strain of 0.5%, and the frequency of 1 s^{-1} were kept constant.

The transmission electron microscopy (TEM) investigations were carried out at the University of Halle. Ultrathin sections, with a thickness of approximately 80 nm, were cut from the center of the parallel zone with a Leica Ultracut Diatome diamond knife (Borsheim, Germany) and subsequently stained with ruthenium tetroxide. Afterwards, the sections were analyzed at an accelerating voltage of 200 kV with a JEOL JEM 2010 (Eching, Germany).

RESULTS AND DISCUSSION

Crystallinity and structure

The first heating scans for the untreated series of injection-molded PP samples are shown in Figure 2, and the corresponding calorimetric parameters (melting enthalpy, crystallinity, melting temperature, and end-set temperature), determined from the thermograms for unannealed and annealed, injection-molded PP samples, are collected in Table III. The dashed line in Figure 2 at 165°C serves to highlight the variation in the

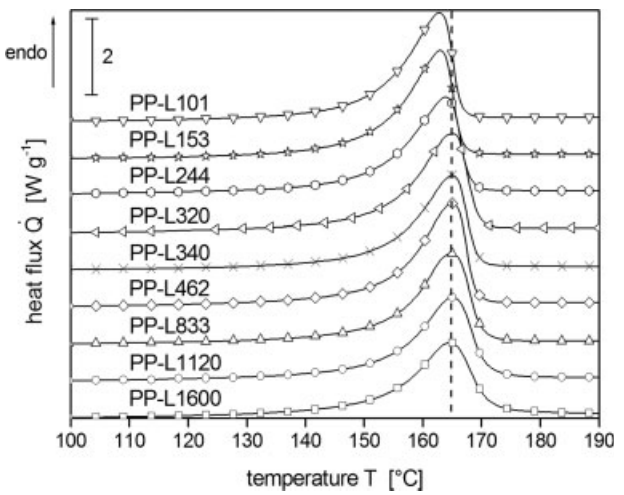

Figure 2 DSC scans of the unannealed PP series with various molecular weights (first heating, 20 K/min heating rate, N_2 atmosphere).

TABLE III
Thermal Properties and Crystallinity of Unannealed and Annealed, Injection-Molded PP Samples (Determined by DSC)

Sample	ΔH_m (J/g)	X_c (%)	T_m (°C)	T_{me} (°C)	$\Delta H_{m,100}$ (J/g)	$X_{c,100}$ (%)	$T_{m,100}$ (°C)	$T_{me,100}$ (°C)	$\Delta H_{m,140}$ (J/g)	$X_{c,140}$ (%)	$T_{m,140}$ (°C)	$T_{me,140}$ (°C)
PP-L1600	81.2	41	164.7	172.5	92.3	47	165.4	173.5	101.3	52	165.5	175.4
PP-L1120	88.9	45	165.0	171.1	93.1	48	165.3	172.1	98.2	50	165.3	171.3
PP-L833	88.9	45	165.3	170.7	92.7	47	165.6	171.6	101.4	52	164.9	171.8
PP-L462	92.9	47	165.3	170.2	96.6	49	165.5	169.9	102.8	52	165.2	169.6
PP-L361	90.0	46	164.9	169.8	94.8	48	164.5	169.1	105.1	54	164.8	169.0
PP-L320	94.3	48	165.2	170.3	96.7	49	163.6	169.0	106.0	54	165.1	169.3
PP-L244	94.5	48	163.9	168.7	95.8	49	163.2	168.1	107.1	55	163.2	167.9
PP-L153	95.8	49	162.5	166.9	94.2	48	162.9	167.5	112.2	57	161.9	166.5
PP-L101	97.1	50	162.5	166.8	100.5	51	162.8	167.3	108.8	56	162.6	167.2

ΔH_m, melting enthalpy; T_m, melting temperature; T_{me}, endset melting temperature; X_c, crystallinity; subscript 100, annealing at a temperature of 100°C for 1 h; subscript 140, annealing at a temperature of 140°C for 1 h.

peak maximum (representing the melting temperature) with changing molecular weight. The DSC thermograms show a characteristic melting behavior of the monoclinic α form of crystals in isotactic polypropylene (iPP), with a monomodal peak at about 162–165°C.[30–34] Samples with molecular weights higher than 244 kg/mol (up to 1600 kg/mol) exhibit no significant difference in the melting point, but the two samples with low molecular weights (<153 kg/mol) exhibit a melting point at the lower temperature of 162°C.

Moreover, there are notable differences in the crystalline fraction as the molecular weight of the samples changed. As expected, the crystallinity sinks from 50% in the case of PP-L101 to 41% for PP-L1600. The reason for this is the presence of a large number of entanglements per chain for the higher molecular weight polymers.

The average number of entanglements per chain [i.e., the entanglement molecular weight (M_e)] can be determined by means of dynamic oscillation rheometry according to the following equation:

$$M_e = \frac{\rho RT}{G_N^0} \quad (1)$$

where R is the universal gas constant (8.314 J mol^{-1} K^{-1}) and ρ is the density of the polymer at temperature T, at which the plateau modulus (G_N^0) was measured.

G_N^0 can be obtained from the frequency at which the minimum of the loss tangent (tan δ_{min}) is located.[35,36]

$$G_N^0 = G'(\upsilon)_{\tan\delta_{min}} \quad (2)$$

Figure 3 shows the master curve of the storage modulus (G') and the loss tangent (tan δ) as a function of frequency for PP-L1600. The tan δ_{min} value is visible at a frequency of 35 s^{-1}, and as a result, $G_N^0 = 450\,000$ Pa can be determined. By means of eq. (1), an entanglement molecular weight of 6730 g/mol has been calculated.

This result is in good agreement with data found in the literature. Eckstein et al.,[37] for instance, recently presented an entanglement molecular weight of 6900 g/mol for iPP with a molecular weight of 871 kg/mol and a polydispersity of 2.4.

With the analyzed entanglement molecular weight for iPP, the number of entanglements per chain can be calculated by the division of the molecular weight of the samples by the entanglement molecular weight. Table I presents the number of entanglements per chain for the PP series. There is a significant difference between the values of the weight-average molecular weight/entanglement molecular weight ratio for the high-molecular-weight samples and the low-molecular-weight samples; in the case of PP-L1600 there are 238 entanglements per chain against 15 for PP-L101.

The entanglements lead to high viscosity in the long polymer chains, so the high-molecular-weight polymers are hindered from forming crystals, and as a result, lower crystallinity exists.

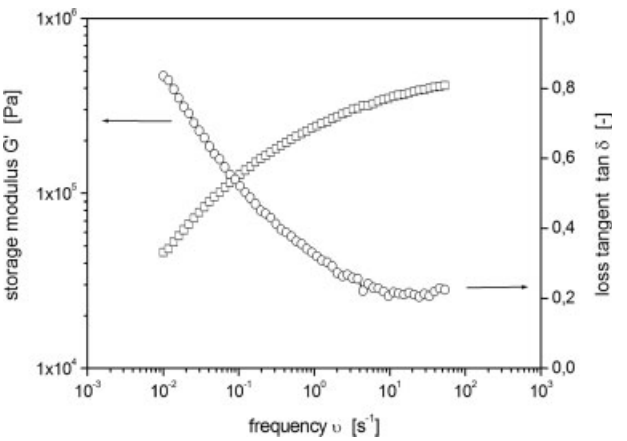

Figure 3 Master curve of G' and tan δ as a function of the frequency for PP-L1600 at a reference temperature of 200°C.

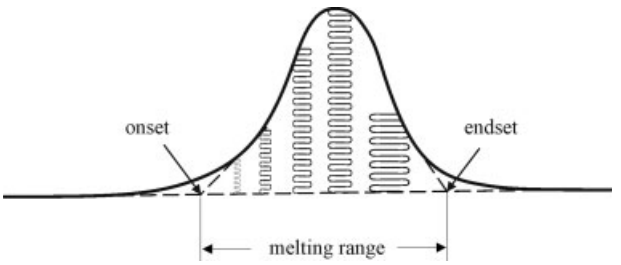

Figure 4 Schematic drawing of the melting zones of crystalline lamellae.

Nevertheless, the crystallinity of the annealed, injection-molded PP dumbbell microspecimens is quantitatively higher as the annealing temperature increases. In the case of high-molecular-weight sample PP-L1600, even an increase in the crystallinity of 11% occurs after annealing at 140°C for 1 h. In contrast, the crystallinity of all other samples increases by approximately 5–7% as a result of an improvement in the crystalline structure during the thermal treatment.

In Figure 2, the melting endotherms of the higher molecular weight samples are broader than those of the lower molecular weight samples. Furthermore, the end-set temperature becomes lower as the molecular weight decreases; this also occurs in the case of thermally treated samples. The beginning of the melting of the crystalline fraction occurs at about 120°C. There, the small, crystalline lamellae begin to melt, and they continue to melt as the temperature increases. At higher temperatures, the thicker and bigger lamellae start to melt completely. Hence, the melting peak characterizes the distribution of the crystalline fraction inside the polymeric sample, as presented schematically in Figure 4. Consequently, the endothermic behavior in the melting range can be considered to analyze and describe the lamellar thickness and distribution.

Evolution of the lamellar thickness and lamellar thickness distribution

According to the relationship stated by Thomson and Gibbs,[38] the average lamellar thickness can be estimated by the relation of the melting temperature (T_m) to the lamellar thickness (L; i.e., the longitudinal dimensions of the crystal) of a polymer as follows:

$$L = \frac{2\varphi_e T_m^0}{\Delta H_f (T_m^0 - T_m)} \tag{3}$$

where T_m^0 is the equilibrium melting temperature of α-phase iPP (464 K[38]), ΔH_f is the melting enthalpy of a perfect crystal (196 J/cm^3 [38]), and ϕ_e is the free surface energy of the end faces at which chains fold (102.9 J/cm^2 [38]).

On the basis of eq. (3), the thickness distribution of crystalline lamellae can by related to the form of the DSC curve with the following equation:

$$\frac{1}{M}\frac{dM}{dL} = \frac{\frac{dE}{dT}(T_m^0 - T_m)^2 \rho_c}{2\varphi_e T_m^0 M} \tag{4}$$

where M is the crystalline mass, and dL is the lamella thickness in the temperature range between T and $T + dT$.

$$\frac{dE}{dT}\frac{1}{M} = \frac{\dot{Q}}{\dot{H}} \tag{5}$$

where ρ_c is the density of the crystal phase (0.936 g/cm^3 [38]), dE is the energy necessary to melt crystalline mass dM in the temperature range between T and $T + dT$, $\dot{H}$ is the heating rate for DSC measurements, and $\dot{Q}$ is the measured heat flux. The heat flux used here is the total heat flux on the DSC thermogram subtracted from a linear baseline.

This relationship of the lamellar thickness distribution and the DSC measurements was described in greater detail by Romankiewicz and Sterzynski.[39]

Figure 5 shows the calculated lamellar thickness distribution of the untreated series of injection-molded PP samples based on the molecular weight. In addition, Table IV presents the average lamellar thickness calculated from the melting temperature and the maximum lamellar thickness determined from the end-set temperature of the unannealed and annealed, injection-molded PP samples. From Figure 5, it is obvious that especially the unannealed samples of low molecular weight (PP-L101 and PP-L244) exhibit thinner lamellae with narrow distributions. In contrast, the other samples (molecular weight = 320–1600 kg/mol) exhibit increasing lamellar thickness and distinctive broadening of the lamellar thickness distribution as

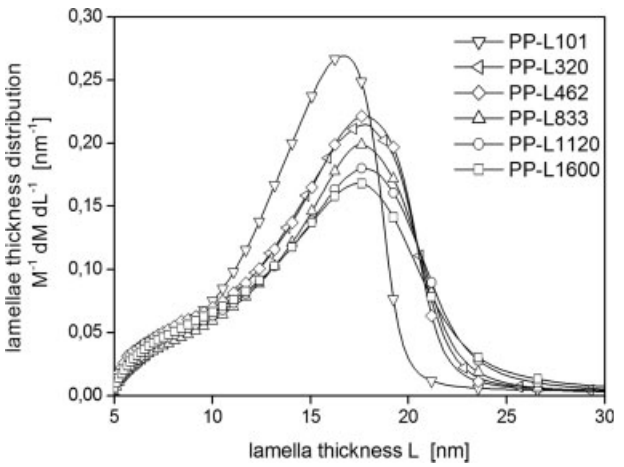

Figure 5 Lamellar thickness distribution of the unannealed PP series with various molecular weights.

TABLE IV
Lamellar Thickness of Unannealed and Annealed, Injection-Molded PP Samples

Sample	L_m (nm)	L_{max} (nm)	$L_{m,100}$ (nm)	$L_{max,100}$ (nm)	$L_{m,140}$ (nm)	$L_{max,140}$ (nm)
PP-L1600	18.5	26.3	19.0	27.8	19.1	31.2
PP-L1120	18.7	24.5	19.0	25.8	19.0	24.7
PP-L833	19.0	24.0	19.2	25.1	18.7	25.4
PP-L462	19.0	23.4	19.1	23.1	18.9	22.8
PP-L361	18.7	23.0	18.4	22.2	18.6	22.1
PP-L320	18.9	23.5	17.8	22.1	18.8	22.5
PP-L244	18.0	21.8	17.5	21.3	17.5	21.1
PP-L153	17.1	20.2	17.3	20.7	16.7	19.9
PP-L101	17.1	20.1	17.3	20.6	17.2	20.5

L_m, average lamellar thickness; L_{max}, maximum lamellar thickness; subscript 100, annealing at a temperature of 100°C for 1 h; subscript 140, annealing at a temperature of 140°C for 1 h.

the molecular weight increases. In particular, the thickness of the thicker lamellae (maximum lamellar thickness), obtained from the evaluation of the end-set temperature, increases drastically with increasing molecular weight. These phenomena have been observed in the past[40,41] and are a result of the reduction in the crystallization rate with increasing molecular weight due to entanglements and viscosity effects, which has been verified previously.

Moreover, the lamellar thickness and, of course, crystallinity also increase because of the increasing mobility of the polymer chains when injection-molded samples are thermally treated at elevated temperatures. Noncrystalline fractions continue to crystallize slowly to improve their crystals inside the superstructure. This effect occurs especially for polymers quickly cooled below the glass-transition temperature (e.g., during the injection-molding process), thereby depressing the crystallization process.

Mechanical properties

The stress–strain behavior of the injection-molded PP dumbbell microspecimens has been analyzed to describe their mechanical behavior. Figures 6 and 7 present detailed plots, from 0 to 30% strain, of the true stress–strain curves for the unannealed and annealed (140°C for 1 h), injection-molded PP samples. Correspondingly, the stress at 8% strain, Young's modulus (tangent modulus) at 0.5% strain, and the strain at break are shown in Table V. The annealed, injection-molded PP samples were only measured up to a strain of 30%, and as a result, no strain at break was determined.

In both Figures 6 and 7, the samples exhibit a stress–strain behavior typical of ductile, semicrystalline polymers. At a low strain, a nearly linear rise in stress characterizes the major pure elastic deformation behavior. This follows more or less distinctively the yielding of the samples, as indicated by a deviation from linearity

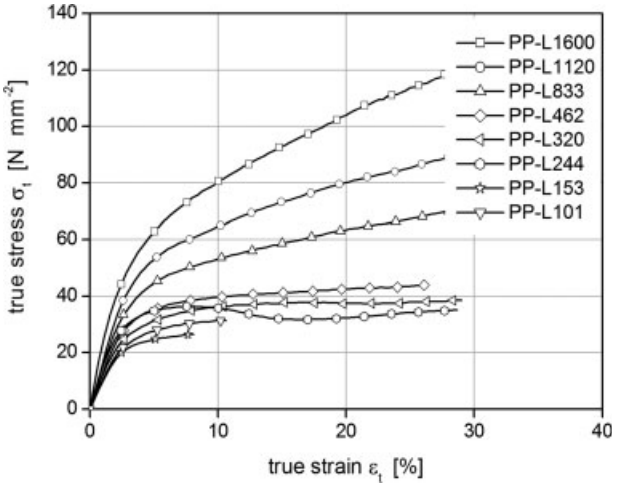

Figure 6 Stress–strain behavior of unannealed, injection-molded PP samples, depending on the molecular weight (strain rate = 3×10^{-4} s^{-1}, contact force = 1 N, temperature = 25°C).

in the stress–strain curve at a strain of about 6%. Here the polymer chains start to slip, and usually necking occurs. As the strain level increases, strain hardening appears until the samples finally break.

In the case of high-molecular-weight samples (from 833 to 1600 kg/mol), no distinctive yielding is detectable, but strain hardening becomes clearly noticeable at about 10% strain. The effect of strain hardening (indicated by a progressive stress–strain curve) becomes more pronounced at higher molecular weights. Similar behavior has been observed by other scientists[13,28] and is discussed in more detail later. Only sample PP-L244 shows distinctive yielding and peaking at 8% strain. Low-molecular-weight samples PP-L101 and PP-L153 break brittlely at strains of about 8 and 11%,

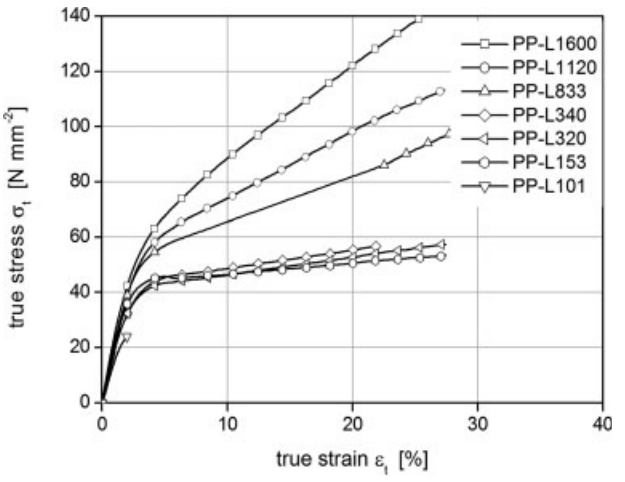

Figure 7 Stress–strain behavior of an injection-molded PP series annealed at 140°C for 1 h, depending on the molecular weight (strain rate = 3×10^{-4} s^{-1}, contact force = 1 N, temperature = 25°C).

TABLE V
Mechanical Properties of Unannealed and Annealed, Injection-Molded PP Samples

Sample	$\sigma_{\varepsilon=0.08}$ (N/mm^2)	$E_{\varepsilon=0.005}$ (N/mm^2)	σ_B (N/mm^2)	ε_B (%)	$\sigma_{\varepsilon=0.08,100}$ (N/mm^2)	$E_{\varepsilon=0.005,100}$ (N/mm^2)	$\sigma_{\varepsilon=0.08,140}$ (N/mm^2)	$E_{\varepsilon=0.005,140}$ (N/mm^2)
PP-L1600	75	2330	158	44	79	2350	83	2320
PP-L1120	61	1480	142	85	67	2030	70	2160
PP-L833	51	1600	121	143	56	1860	NA	NA
PP-L462	39	1350	77	208	47	1680	45	2000
PP-L361	36	1560	NA	NA	NA	NA	47	1880
PP-L320	35	1300	67	216	45	1670	45	1820
PP-L244	36	1570	NA	NA	44	1520	46	1720
PP-L153	27	1340	NA	NA	36	1020	NA	NA
PP-L101	30	1270	32	11	NA	1370	NA	1560

ε_B, strain at break; $E_{\varepsilon=0.005}$, Young's modulus at 0.05% strain; NA, not available; σ_B, stress at break; $\sigma_{\varepsilon=0.08}$, stress at 8% strain; subscript 100, annealing at a temperature of 100°C for 1 h; subscript 140, annealing at a temperature of 140°C for 1 h.

respectively. Hence, there is a minimum molecular weight of 153 kg/mol, below which polymeric materials are brittle. From the literature,[42] it is known that the ductile-to-brittle transition usually appears when the molecular weight is twice the entanglement molecular weight. This theory is explained by the fact that the entanglements between lamellae are responsible for carrying a large amount of the stress during the tensile test, so the absence of entanglements strongly affects the fracture behavior.

Based on an entanglement molecular weight of 6700 g/mol (calculated previously with viscoelastic data), the critical molecular weight of iPP is about 13,400 g/mol, that is, much lower than the molecular weights of the brittle samples, although in contrast the number of entanglements per chain of those samples is lower than that of the high-molecular-weight samples. As a result, other factors must play a role in the transition from ductile-to-brittle behavior as the molecular weight decreases.

The fact that low-molecular-weight samples PP-L101 and PP-L153 rupture just after yielding and fail to exhibit necking in tensile tests is assumed to be due to early (at low deformation) stretching of the short molecular chains to their maximum and the breaking of few entanglements per chain.

To understand the stress–strain behavior of the injection-molded PP series, the morphological structure should be considered. As known from DSC measurements, the crystallinity of low-molecular-weight PP samples is higher than that of high-molecular-weight samples, and the lamellar thickness increases, most notably in the case of thicker lamellae, as the molecular weight increases. As a result, the amorphous fraction between the lamellae increases with the molecular weight. Additionally, the number of entanglements per chain increases as the molecular weight increases.

From morphological studies, it is most observable by TEM analysis of the unannealed PP samples that the structure of the dumbbell microspecimens changes, depending on the molecular weight. The low-molecular-weight samples clearly exhibit a spherulitic structure in the core, as it is recognizable by the sporadic, cross-hatched structures in Figure 8(a). In contrast,

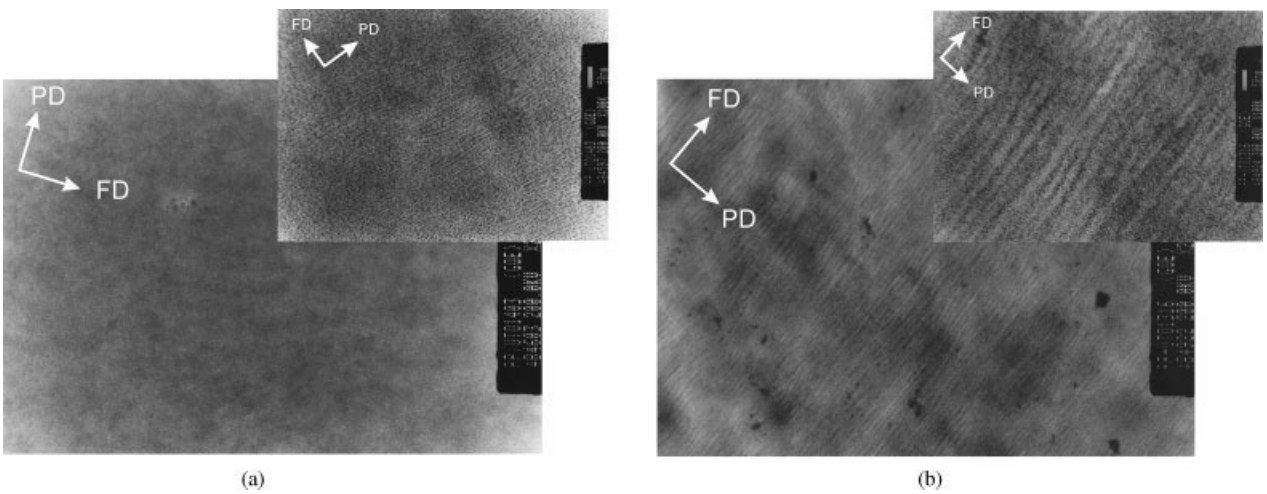

Figure 8 TEM micrographs of PP-L101 and PP-L1600 dumbbell microspecimens with magnifications of 20,000× and 100,000× (FD = direction of the flow, PD = perpendicular to the direction of the flow).

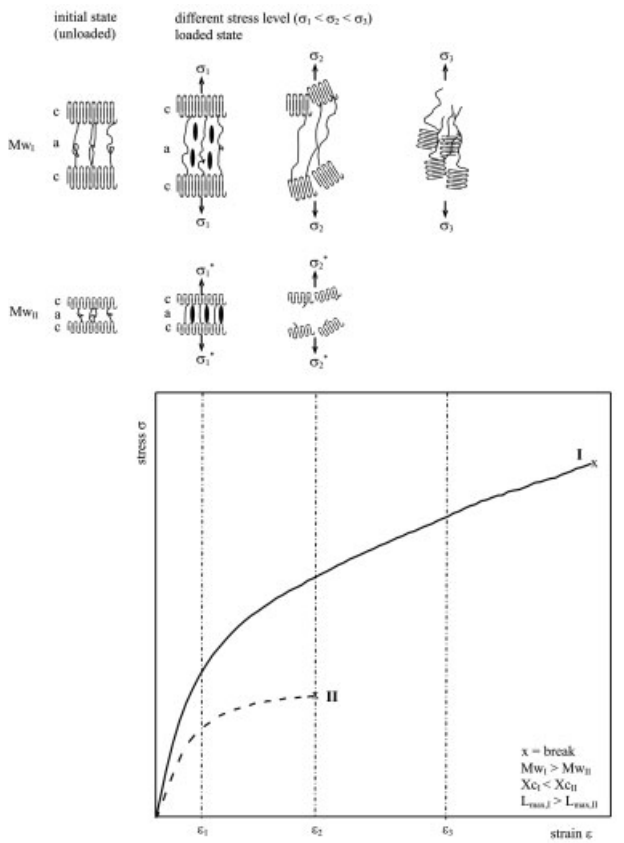

Figure 9 Schematic illustration of the deformation behavior (c = crystalline, a = amorphous).

highly oriented, shear-induced structures (shish kebab) can be observed as the molecular weight increases, as presented in Figure 8(b). More details on the formation of the morphology depending on the molecular weight of the samples and on the shear rate have been published recently.[43]

On the basis of these results and our current understanding, a schematic model of the structural changes of low-molecular-weight and high-molecular-weight polymers during deformation can be postulated, as shown in Figure 9.

First, the elongation of the samples in the tensile direction causes stretching of the amorphous phase. This process is purely elastic; once the load on the sample is removed, it fully recovers. When the semicrystalline polymer is further deformed, plastic yielding occurs, at which crystallite sliding takes places. Thus, the lamellae start to orientate themselves parallel to the deformation direction; correspondingly, interlamellar slipping occurs, coupled with the unfolding of the lamellae until the ultimate break. Peterlin[15–18] described this mechanism as the breaking of the lamellae into microblocks and their reorganization in microfibrils accompanied by interlamellar separation and insertion of unfolded molecular chains into the amorphous fraction. As a result, strain hardening occurs.

On the basis of the explained deformation processes, the difference in the stress–strain behavior of the different molecular weights of untreated and thermally treated injection-molded samples can be explained.

Young's modulus corresponds to the initial response of the material to energy input (strain) and is attributed to the stiffness of the material at low deformation. Therefore, from the point of view of material science, it is decisive how stress will be transmitted through the crystalline fraction and mainly the amorphous fraction.

Here, Young's modulus is estimated as the tangent modulus at a strain of 0.5%. Figure 10 shows that Young's modulus increases as the molecular weight increases in a nearly linear fashion. Additionally, at the same molecular weight, Young's modulus is higher as the crystallinity increases within the same sample. Increasing crystallinity is caused by annealing at higher temperatures (see Fig. 11). However, when we compare Young's modulus within the PP series, the higher molecular weight samples, which exhibit less crystallinity, are stiffer than the low-molecular-weight samples with greater crystalline fractions. Therefore, the known and often reported phenomenon[13,23,44] that Young's modulus usually rises continuously as the crystallinity increases is only correct with respect to one defined-molecular-weight sample. The high stiffness of up to 2300 N/mm^2 for the PP samples is caused by an existing shish-kebab structure. As observed by TEM analysis and presented in more detail previously,[43] the low-molecular-weight PP samples exhibit non-shish-kebab structures, but as the molecular weight and shear rate increases, the number of shish kebabs increases.

Because of their architecture, the shish kebabs can sustain most of the stress. The shishes, consisting of fibrous crystals penetrating the texture, are responsi-

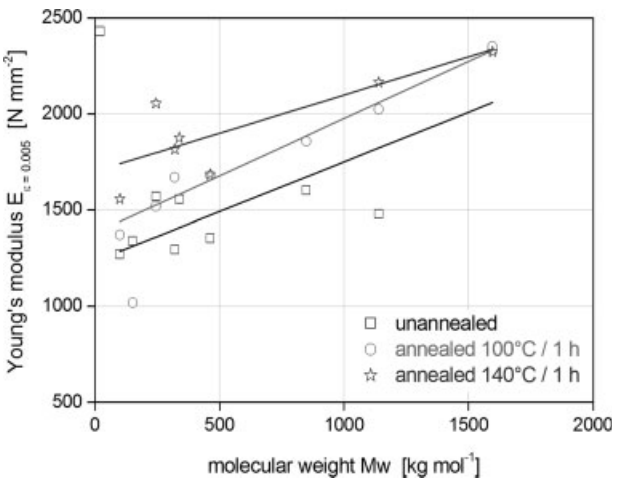

Figure 10 Dependence of Young's modulus on the molecular weight of unannealed and annealed, injection-molded PP samples.

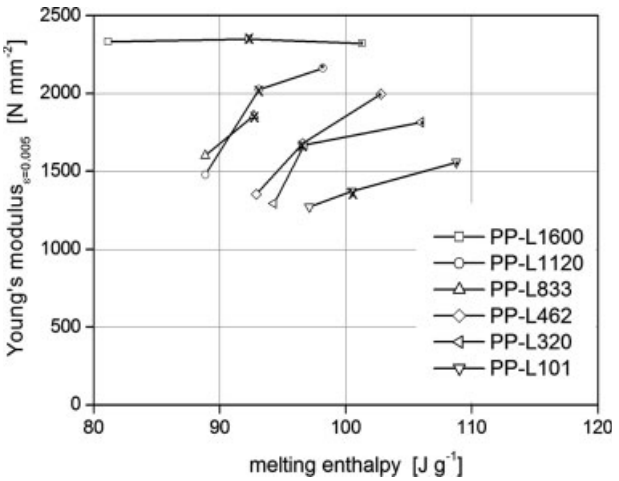

Figure 11 Dependence of Young's modulus on the melting enthalpy of unannealed and annealed, injection-molded PP samples. Crossed symbols indicate 100°C for 1 h, and dotted symbols indicate 140°C for 1 h.

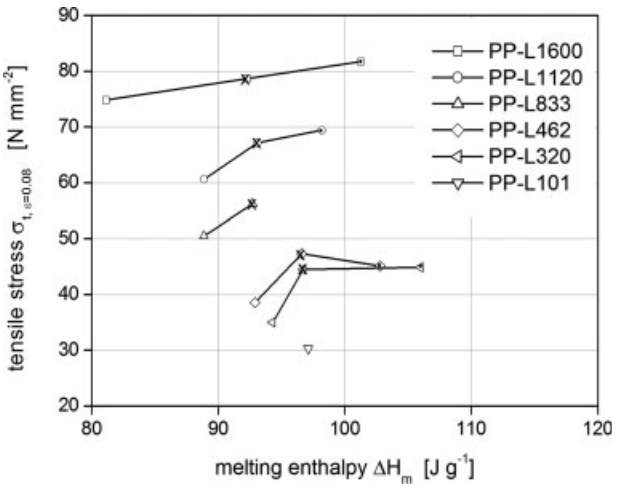

Figure 13 Dependence of the tensile stress at 8% strain on the melting enthalpy of unannealed and annealed, injection-molded PP samples. Crossed symbols indicate 100°C for 1 h, and dotted symbols indicate 140°C for 1 h.

ble for high stiffness in the direction of flow (i.e., the direction of tension), and the kebabs, lamellae around the shishes, are responsible for high stiffness transverse to the direction of flow.

However, there is another reason for the high stiffness of the PP samples. The stiffness of samples annealed at high temperatures is greater than that of unannealed samples, although the proportion of shish-kebab structures either remains the same or is probably even smaller after the annealing of the samples. Therefore, another factor must be involved, and it seems to be the mobility of the amorphous fraction. This can be explained by the different dynamic mechanical responses of the PP samples before and after annealing, as measured by dynamic mechanical analysis (DMA) and described later.

Figures 12–14 show the behavior of the tensile strength based on the molecular weight, melting enthalpy (corresponds to crystallinity), and lamellar thickness. The stress at a strain of 8% (i.e., the yield point of PP-L244) is used as the tensile strength, because not all the samples show extensive yielding.

Similarly to the stiffness, which is dependent on the molecular weight, the tensile strength increases proportionally as the molecular weight increases. Furthermore, when we compare the tensile strength dependence on the crystallinity for the same molecular weight, we find that the tensile strength increases as

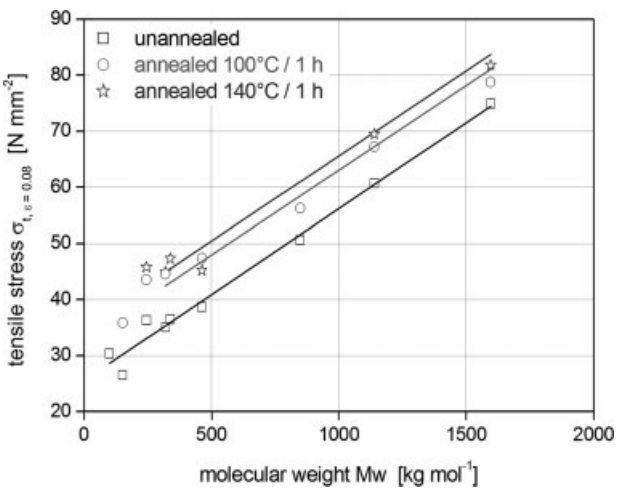

Figure 12 Dependence of the tensile stress at 8% strain on the average molecular weight of unannealed and annealed, injection-molded PP samples.

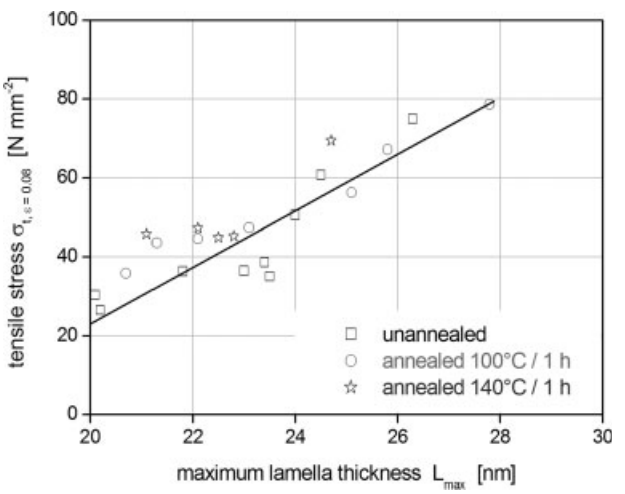

Figure 14 Tensile stress at 8% strain as a function of the maximum lamellar thickness.

the crystallinity increases, as shown in Figure 13. When we consider that the crystallinity analyzed by DSC is lower for high-molecular-weight samples than for lower molecular weight samples, the tensile strength of PP-L1600 should be lower than that of PP-L101. However, the results presented in Figure 13 show the opposite. As a result, the well-known, basic rule, that the stiffness and tensile strength increase with increasing crystallinity, can be applied only for samples with the same molecular weight and is not transferable to samples with different molecular weights.

The highly oriented shish-kebab structure also affects the tensile strength and strain hardening at higher deformation, as does the stiffness. Although the number of shish kebabs is probably not influenced by the thermal treatment, increases in the strength and strain hardening after annealing indicate that an additional factor governs the tensile strength.

The results seem to be governed mainly by the lamellar thickness and lamellar thickness distribution. This explanation can be affirmed by a linear relation between the tensile strength and maximum lamellar thickness, calculated from the DSC results, as shown in Figure 14. Therefore, thicker lamellae, which evolve from long molecular chains, can sustain large deformations. This again explains why the tensile strength is higher after the thermal treatment of the samples according to a comparison of the tensile stress values at 8% strain for the samples of the same molecular weight, as shown in Figure 13.

Similar behavior was first observed by Young[45] for polyethylene (PE). He announced that the tensile yield stress is activated by screw dislocation of the lateral surface of crystalline lamellae, indicating that the lamellar thickness considerably influences the yield stress. Schrauwen et al.[14] confirmed this theory, finding that yield stress depends on the lamellar thickness. They found a fair correlation between the yield stress measured in PE and that predicted by a mechanism involving the propagation of screw dislocation. Séguéla[46] showed for PE and PP that the tensile yield stress depends on the lamellar thickness, rather than the crystallinity. He found the result to be consistent with Young's model of dislocation.

In addition to the increase in the tensile stress, a more pronounced strain hardening can be observed as the lamellar thickness increases (see Figs. 6 and 7). The reason for this is that the slipping and orientation of lamella become more difficult as the thickness increases. Moreover, additional unfolding of longer molecular chains is more complicated in the case of high-molecular-weight polymers. This explanation is confirmed by the stress–strain behavior of the samples annealed at 140°C for 1 h, as shown in Figure 7. When the samples of the same molecular weight are compared before and after annealing, strain hardening is more pronounced for the thermally treated samples than for the untreated samples; this is due to growing lamellar thickness during the annealing procedure.

Spectacularly, high-molecular-weight sample PP-L1600 even achieves an unusual high true tensile stress of up to 158 N/mm^2. This impressive tensile strength, 3 times higher than the known tensile strength of commercially available PP, is atypical of PP. As far as we know, such high tensile strength for injection-molded, dumbbell specimens has not been reported in the literature until now.

Prox and Ehrenstein[47] found for PP with a molecular weight of 470 kg/mol a maximum tensile strength of about 80 N/mm^2 but a low strain at break of about 32%. They studied injection-molded PP dumbbell specimens within a molecular weight range of 240–653 kg/mol and under extreme processing conditions, such as a high injection speed (180 mm/s) and low melt (160°C) and mold temperatures (25°C), to obtain self-reinforcement. Analyzing the dependence of the molecular weight on the mechanical properties, they found a peak improvement of the tensile strength at an average molecular weight of 470 kg/mol.

Furthermore, Kalay and Bevis[24] observed an increase in Young's modulus of moldings produced by shear-controlled, orientation injection molding. By controlling the processing parameters, they could control and enhance the stiffness without the loss of tensile strength. They reported a maximum increase in Young's modulus of up to 2600 N/mm^2 and a peak tensile strength of 55 N/mm^2 for moldings with iPP with an average molecular weight of 460 kg/mol, but this was linked to a reduction in the strain at break of about 55%.

Albano et al.[48] produced plaques from iPP within a molecular weight range of 210–800 kg/mol with conventional injection molding. They studied the influence of the molecular weight and thermal history on the mechanical properties and obtained samples with a tensile strength of 58 N/mm^2 and a strain at break of about 90% but with a low Young's modulus of about 830 N/mm^2.

However, extremely strong and stiff PP with a stiffness of up to several kilonewtons per square millimeter is known only in highly (biaxial) drawn and anisotropic PP films and fibers produced by special processing techniques. Here the disadvantage is the low obtainable ultimate strain: less than approximately 10%.

Viscoelastic properties

Semicrystalline polymers show several types of relaxation phenomena that can be detected by DMA. As a result of certain molecular motions, a storage modulus depression or a loss modulus peak appears on the mechanical relaxation curve.

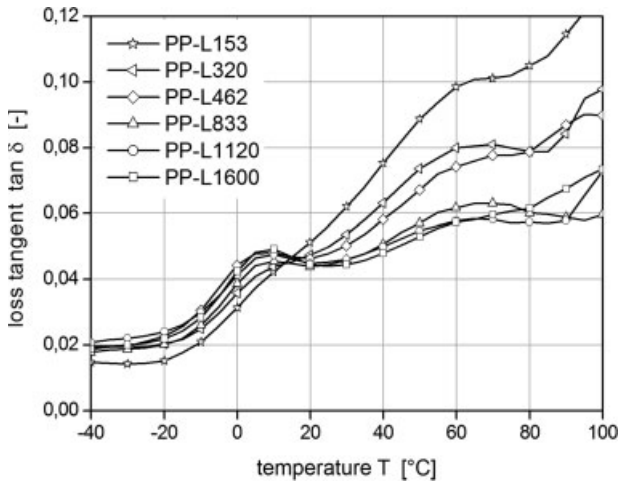

Figure 15 Tan δ as function of temperature for unannealed, injection-molded PP samples with various molecular weights (static strain = 1%, dynamic strain = 0.1%, frequency = 1 s^{-1}, heating rate = 5 K/min).

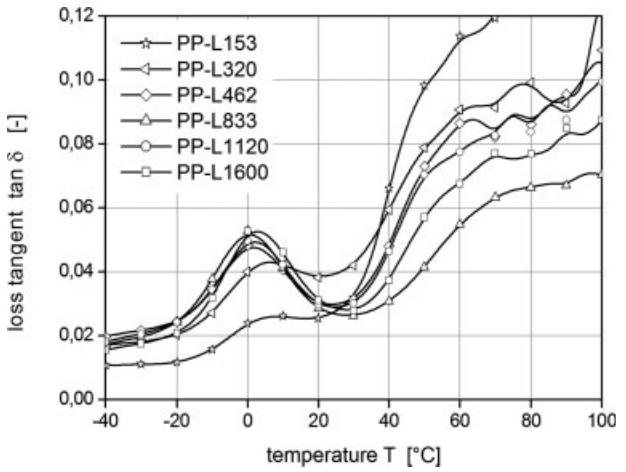

Figure 16 Tan δ as a function of temperature for injection-molded PP samples annealed at 140°C for 1 h with various molecular weights (static strain = 1%, dynamic strain = 0.1%, frequency = 1 s^{-1}, heating rate = 5 K/min).

In the case of iPP, dynamic mechanical relaxation processes can be observed from −50°C to nearly the melting temperature. Typically for PP, there are three different relaxation processes due to molecular motions activated by thermal energy.[49–52] First, very short range motions, such as methyl group rotation in side-chain ends, occur at approximately −50°C; this motion is termed the γ-relaxation process. The β-relaxation process at higher temperatures of about 0°C is the dominant relaxation and can be attributed to the transition from the glassy state to the rubbery state in amorphous polymers, but it should be taken into account that the amorphous region in a crystalline polymer is different from that in a completely amorphous polymer, in that the molecular motions of the amorphous phase are constrained by the crystallites. In the temperature region close to the melting temperature, the α-relaxation process takes place because of motions in the interphase of crystallites. Although the reason for this α-relaxation process is still controversial, it is well documented[49–51] that the α relaxation is strongly affected by orientation; on the one hand, this effect occurs primarily in temperature regions above 30°C, and on the other hand, it is affected by the length of chain foldings at the interphase, which again depends on the molecular weight and occurs at about 100°C.

Observing all three relaxation processes, we performed measurements from the very low temperature of −50°C up to 140°C. Detailed plots, ranging from −40 to 100°C, of the storage modulus (E') and tan δ as a function of the temperature for a representative selection of the unannealed and annealed, injection-molded PP samples are presented in Figures 15–18. Both Figures 15 and 16 show a very weak and distinctive γ relaxation due to fewer CH_3 motions.

In contrast, in the range of the β relaxation, a vast peak can be observed between 0 and 10°C of the tan δ curve (Fig. 15), which corresponds to the glass-transition temperature of iPP. From there, the magnitude of the β relaxation was determined after the subtraction of a fitted, linear baseline.

As shown in Figures 15, 16, and 19, a marked difference in the magnitude of the β relaxation exists when we compare samples with different molecular weights. It is demonstrated in Figure 19 that the magnitude of the β relaxation increases rapidly with increasing molecular weight toward asymptotic limits, which are reached at magnitudes of about 0.015 for the unannealed samples and 0.038 for the

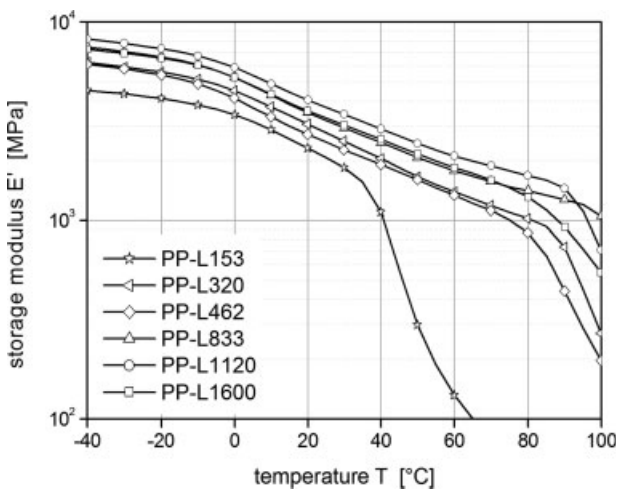

Figure 17 E' as a function of temperature for unannealed, injection-molded PP samples with various molecular weights (static strain = 1%, dynamic strain = 0.1%, frequency = 1 s^{-1}, heating rate = 5 K/min).

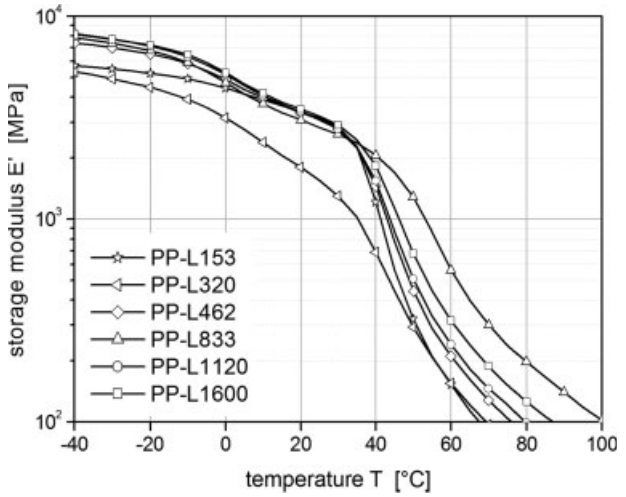

Figure 18 E' as a function of temperature for PP samples annealed at 140°C for 1 h with various molecular weights (static strain = 1%, dynamic strain = 0.1%, frequency = 1 s^{-1}, heating rate = 5 K/min).

annealed (140°C for 1 h) samples. Despite this, only a weak difference in the maximum magnitude of the β relaxation can be observed between the unannealed samples and the samples annealed at 100°C for 1 h. The reason for this seems to be the fact that minor changes in the morphological structure occur when an annealing temperature of 100°C, which is below the crystallization temperature of the PP samples, is used. In contrast, when the injection-molded PP samples are annealed at temperatures of 140°C, which is above the crystallization temperature of the PP samples (~120°C), postcrystallization is promoted, and as a result, the nanostructure is changed.

In fact, a decrease in the mechanical relaxation of the β process is associated with a reduction in the mobility of the polymer chains in the amorphous phase.[49,51,52] On the one hand, the reason may be lower amounts of the amorphous fraction, but this explanation is not totally consistent with the results found in Figure 20. The magnitude of the β relaxation increases as the content of the amorphous fraction decreases after the annealing of the injection-molded PP samples. For example, when we compare the magnitude of the β relaxation and the amount of the amorphous fraction of injection-molded sample PP-L320 before and after annealing, the magnitude of the β relaxation increases 4 times [the β relaxation is 0.005 and 0.022 before and after annealing (140°C for 1 h)], although the content of the amorphous fraction decreases from 52 to 46%.

However, when we compare the magnitudes of the β relaxation for the untreated, low-molecular-weight sample PP-L101 and high-molecular-weight sample PP-L1600, it turns out, as expected, that the β relaxation is higher (0.002 and 0.015 for PP-L101 and PP-L1600, respectively) with a higher content of the amorphous fraction (51 and 58% for PP-L101 and PP-L1600, respectively). Therefore, the way in which the content of the amorphous phase is changed should be taken into account in this explanation.

On the other hand, another reason may be a change in the molecular packing in the amorphous phase. Denser packing of the molecular chains leads to a reduction in the molecular motion. As can be observed in Figure 19, when we compare the magnitudes of the β relaxation in the unannealed and annealed (mainly at 140°C for 1 h) samples, an obvious rise in the magnitude of the β relaxation can be noticed, although there is a reduction in the amorphous fraction after the annealing procedure. Furthermore, stiffening of the

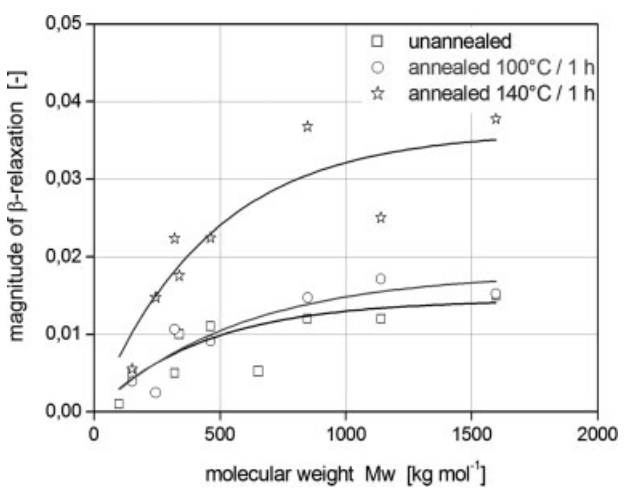

Figure 19 Dependence of the magnitude of the β relaxation for unannealed and annealed, injection-molded PP samples with various molecular weights.

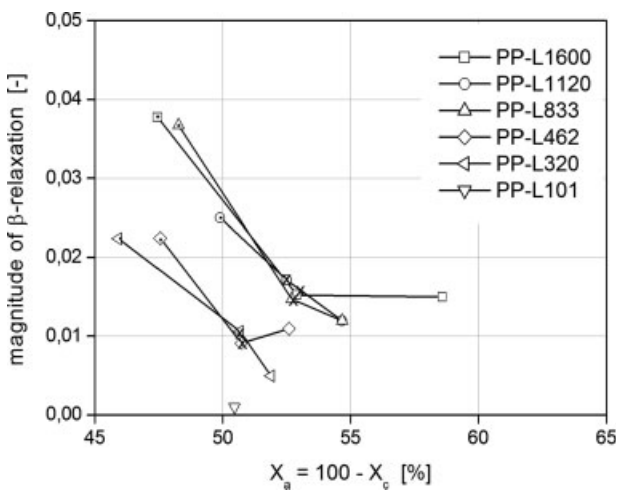

Figure 20 Dependence of the magnitude of the β relaxation on the amorphous fraction for unannealed and annealed, injection-molded PP samples (X_a = amorphous fraction, X_c = crystalline fraction). Crossed symbols indicate 100°C for 1 h, and dotted symbols indicate 140°C for 1 h.

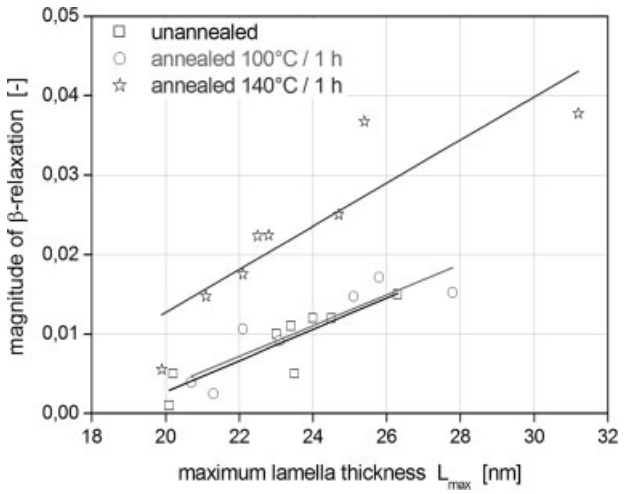

Figure 21 Dependence of the magnitude of the β relaxation on the maximum lamellar thickness for unannealed and annealed, injection-molded PP samples.

amorphous components can usually be observed after annealing.[53] Therefore, both the amount of the amorphous phase and the structure of the amorphous fraction, mainly between the lamellae, govern the relaxation process. In particular, within the thicker lamellae, there are considerably more mobile interlamellar amorphous components, which are not limited in their motions by crystallites. This implies a rapid rise in the magnitude of the β relaxation as a function of the maximum lamellar thickness, as shown in Figure 21.

Moreover, a marked rise in the magnitude of the β relaxation appears for all samples of the PP series thermally treated at 140°C for 1 h. This leads to the assumption that considerably freer molecular mobility exists because of the reorganization of the structure, which can be further supported by the fact that a shifting of the tan δ peak to 0°C from 10°C is observable when Figures 15 and 16 are compared. A reduction in the glass-transition temperature is generally caused by an increase in the free volume, consequently enhancing the spatial mobility of the molecules and leading to a rubberlike behavior at lower temperatures. As a further result, the stiffness of the material is influenced considerably by the mobility of the amorphous components, as shown in Figure 22. In fact, a linear correlation between Young's modulus and the magnitude of the β relaxation can be observed.

Of course, the mobile, interlamellar amorphous fraction also influences the α-relaxation process intensively. In Figure 15, the α relaxation clearly shows a broad peak with a weak shoulder at about 60°C. Thus, tan δ increases at about 30°C, but this is more gradual for high-molecular-weight samples. In contrast, the low-molecular-weight sample shows a marked rise, beginning at about 20°C, with a much more progressive slope than that of the curves of high-molecular-weight PP. Such behavior can be attributed to crystal–crystal sliding. This mechanism requires mobility in the interlamellar regions; otherwise, the movement of crystals is hindered.

However, the untreated, injection-molded PP specimens in Figure 15 show that the samples with a more mobile amorphous fraction exhibit a smaller α-relaxation peak. For example, PP-L1600 exhibits a pronounced β-relaxation peak at 10°C, but in contrast, almost no mechanical response in the α-relaxation range can be recognized.

Distinctive α-relaxation behavior, as can be observed for the lower molecular weight samples in Figure 15, is well known for oriented samples, for example, because of special drawing processes.[50,51,54] This is due to the fact that molecules arranged parallel to the direction of deformation can slip more easily.

Pluta et al.,[51] for instance, investigated iPP samples compressed in a channel die at 110°C up to a compression ratio of 6.6. They found that less deformation of iPP samples already influences the α-relaxation process and is noticeable by a marked increase in the tan δ curve at temperatures above 30°C. The main deformation mechanisms found were crystallographic slips along the chain direction.

Moreover, for highly zone-drawn PP fibers, Suzuki et al.[50] noticed a loss in the β relaxation and a correspondingly distinctive α relaxation starting at 20°C. To that, they attributed an increase found in the storage modulus as the drawing ratio increased. They implied that intercrystalline bridges connect the crystal regions longitudinally and cause sliding processes.

de Candia et al.[54] confirmed Suzuki's finding, also finding that the modulus is substantially a function of the drawing degree in the case of two-step drawn iPP. Additionally, they obtained increases in the α-relaxation process for highly drawn PP fibers, starting at 40°C.

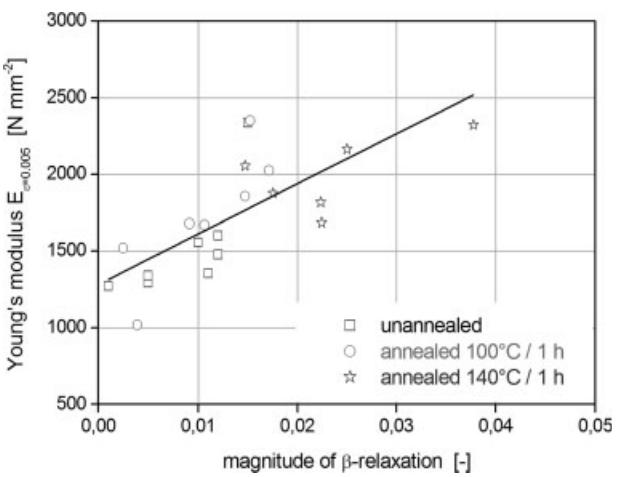

Figure 22 Young's modulus as a function of the magnitude of the β relaxation.

On the basis of these findings and information available on the α-relaxation process, there have to be additional morphological effects hindering the slipping process as the molecular weight increases. As known from a morphological investigation, there are highly oriented shish kebabs possessing high stiffness and strength due to extended molecular chains lying parallel to each other. Kebabs are formed radially around the oriented molecular chains, which can interlock the shish kebabs, thus strongly limiting motion. Therefore, the shish kebabs, increasing in number with increasing molecular weight and shear rate, cause an observable decline in the α relaxation.

This explanation is further supported by the fact that the rise of tan δ in the α-relaxation process, starting at about 30°C, appears more distinctly, and the drastic E' drop shifts to the lower temperature of 40°C; this can be seen by a comparison of the unannealed and annealed, injection-molded PP samples in Figures 17 and 18. At 80°C, E' of high-molecular-weight sample PP-L1600 decreases from 1200 N/mm^2 in the case of the unannealed samples to 120 N/mm^2 for the annealed samples, or about 100 times. During the annealing of the PP samples, the molecules are thermally stimulated to form thermodynamically stable structures, preferably the folding of chains to spherulites in the case of linear polymers, as a result of which the shish-kebab structure is partially dissolved. This reorganization of structure leads to a reduction in orientation and furthermore to easier crystal–crystal sliding processes.

CONCLUSIONS

The study of the mechanical deformation behavior of the injection-molded PP specimens, depending on their molecular weight, has found that the stiffness and tensile strength increase as the molecular weight increases. PP-L1600 exhibits a true tensile strength of 158 N/mm^2, 3 times higher than the known tensile strength of commercially available PP. The reason for this is the existence of highly oriented shish-kebab structures and, in addition, an increase in the lamellar thickness as the molecular weight increases. For the existing superstructure, the maximum lamellar thickness governs the tensile stress as well as the strain hardening effect, rather than the overall crystallinity. The recognized phenomenon that the tensile strength and stiffness usually rise continuously as the crystallinity increases is correct only for one defined molecular weight.

Young's modulus (i.e., stiffness) of injection-molded, dumbbell microspecimens is determined by the mobility of the amorphous fraction. The magnitude of the β relaxation, measured by DMA, indicates the mobility of the amorphous phase; that is, the packing of the amorphous phase between the lamellae is more important than the overall content of the amorphous phase.

Furthermore, the injection-molded PP samples rupture at lower strain as the molecular weight increases, with the exception of injection-molded specimens PP-L101 and PP-L153, which already break at ultimate strains of 8 and 11%. As a result, a ductile-to-brittle transition occurs when the molecular weight passes 153 kg/mol.

Altogether this investigation of mechanical properties shows that especially the interlamellar amorphous fraction and lamellar thickness, as well as highly oriented structures (e.g., shish kebab), mainly govern the mechanical response of the samples and define their structural behavior. If differences in the morphology exist, then changes also arise in the mechanical and viscoelastic properties.

References

1. Jay, F.; Haudin, J. M.; Monasse, B. J Mater Sci 1999, 34, 2089.
2. Zhu, P.; Edward, G. Polymer 2004, 45, 2603.
3. Seki, M.; Thurman, D. W.; Oberhauser, J. P.; Kornfield, J. A. Macromolecules 2002, 35, 2583.
4. Haudin, J. M.; Duply, C.; Monasse, B.; Costa, J. L. Macromol Symp 2002, 185, 119.
5. Somani, R. H.; Yang, L.; Sics, I.; Hsiao, B. S.; Pogadina, N. V.; Winter, H. H.; Agarwal, P.; Fruitwala, H.; Tsou, A. Macromol Symp 2002, 185, 105.
6. Pantani, R.; Speranza, V.; Sorrentino, A.; Titomanlio, G. Macromol Symp 2002, 185, 293.
7. Ren, W. Colloid Polym Sci 1992, 270, 943.
8. Piccarolo, S. J Macromol Sci Phys 1992, 31, 501.
9. Eder, G.; Janeschitz-Kriegl, H.; Krobath, G. Colloid Polym Sci 1988, 266, 1087.
10. de Carvalho, B.; Bretas, R. E. S. J Appl Polym Sci 1998, 68, 1159.
11. Varga, J. J Mater Sci 1992, 27, 2557.
12. Varga, J.; Karger-Kocsis, J. J Polym Sci Part B: Polym Phys 1996, 34, 657.
13. Schrauwen, B. A. G.; Breemen, L. C. A.; Spoelstra, A. B.; Govaert, L. E.; Peters, G. W. M.; Meijer, H. E. H. Macromolecules 2004, 37, 8618.
14. Schrauwen, B. A. G.; Janssen, R. P. M.; Govaert, L. E.; Meijer, H. E. H. Macromolecules 2004, 37, 6069.
15. Peterlin, A. J Mater Sci 1971, 6, 490.
16. Peterlin, A. Int J Fract 1975, 11, 761.
17. Peterlin, A. Colloid Polym Sci 1987, 265, 357.
18. Peterlin, A. Polym Eng Sci 2004, 3, 183.
19. Samuels, R. J. Structured Polymer Properties; Wiley: New York, 1974.
20. Naundorf, I.; Osterloh, S.; Fischer, G. Plastverarbeiter 1995, 45, 18.
21. Naundorf, I.; Osterloh, S.; Fischer, G. Plastverarbeiter 1995, 45, 120.
22. Kantz, M. R.; Newman, H. D.; Stigale, F. H. J Appl Polym Sci 1972, 16, 1249.
23. van der Meer, D. W.; Pukanszky, B.; Vansco, G. J. J Macromol Sci Phys 2002, 41, 1105.
24. Kalay, G.; Bevis, M. J. J Polym Sci Part B: Polym Phys 1997, 35, 241.
25. Kalay, G.; Bevis, M. J. J Polym Sci Part B: Polym Phys 1997, 35, 265.
26. Isayev, A. I.; Chan, T. W.; Shimojo, K.; Gmerek, M. J Appl Polym Sci 1995, 55, 807.
27. Isayev, A. I.; Chan, T. W.; Gmerek, M.; Shimojo, K. J Appl Polym Sci 1995, 55, 821.

28. Fujiyama, M.; Wakino, T.; Kawasaki, Y. J Appl Polym Sci 1988, 35, 29.
29. Al-Hai Ali, M.; Roffel, B.; Weickert, G.; Bettlem, B.AIChE 2006, 52, 1866.
30. Aboulfaraj, M.; Ulrich, B.; Dahoun, A.; G'Sell, C. Polymer 1993, 34, 4817.
31. O'Kane, W. J.; Young, R. J.; Ryan, A. J. J Macromol Sci Phys 1995, 34, 427.
32. Lima, M. F. S.; Vasconcellos, M. A. Z.; Samios, D. J Polym Sci Part B: Polym Phys 2002, 40, 896.
33. Lu, H.; Qiao, J.; Xu, Y.; Yang, Y. J Appl Polym Sci 2002, 85, 333.
34. Heeley, E. L.; Maidens, A. V.; Olmsted, P. D.; Bras, W.; Dolbnya, I. P.; Fairclough, J. P. A.; Terrill, N. J.; Ryan, A. J. Macromolecules 2003, 36, 3656.
35. Wu, S. J Polym Sci Part B: Polym Phys 1987, 25, 557.
36. Wu, S. Polymer 1987, 28, 1144.
37. Eckstein, A.; Suhm, J.; Friedrich, C.; Maier, R. D.; Sassmannshausen, J.; Bochmann, M.; Mülhaupt, R. Macromolecules 1998, 31, 1335.
38. Bershtein, V. A.; Egorov, V. M. Differential Scanning Calorimetry of Polymers: Physics, Chemistry, Analysis; Ellis Horwood: London, 1994.
39. Romankiewicz, A.; Sterzynski, T. Macromol Symp 2002, 180, 241.
40. Heck, B.; Hugel, T.; Iijima, M.; Sadiku, E.; Strobly, G. New J Phys 1999, 1, 17.1.
41. Dötsch, T.; Pollard, M.; Wilhelm, M. J Phys: Condens Matter 2003, 15, 923.
42. Barham, P. J. In Materials Science and Technology: A Comprehensive Treatment; Cahn, R. W.; Haasen, P.; Kramer, E. J., Eds.; VCH: Weinheim, 1993; Vol. 12.
43. Stern, C.; Frick, A. R.; Weickert, G.; Michler, G. H.; Henning, S. Macromol Mater Eng 2005, 290, 621.
44. O'Kane, W. J.; Young, R. J. J Mater Sci Lett 1995, 14, 433.
45. Young, R. J. J. Philos Mag 1974, 30, 85.
46. Séguéla, R. J Polym Sci Part B: Polym Phys 2002, 40, 593.
47. Prox, M.; Ehrenstein, G. W. Kunststoffe 1991, 81, 11.
48. Albano, C.; Sciamanna, R.; Kaiser, D.; Delgado, G. Rev Facultad Ing 2001, 16, 69.
49. McCrum, N. G.; Read, B. E.; Williams, G. Anelastic and Dielectric Effects in Polymeric Solids; Wiley: New York, 1967.
50. Suzuki, A.; Sugimura, T.; Kunugi, T. J Appl Polym Sci 2001, 81, 600.
51. Pluta, M.; Bartczak, Z.; Galeski, A. Polymer 2000, 41, 2271.
52. Jourdan, C.; Cavaille, J. Y.; Perez, J. J Polym Sci Part B: Polym Phys 1989, 27, 2361.
53. Michler, G. H. Kunststoff-Mikromechanik—Morphologie, Deformations- und Bruch-Mechanismen; Hanser: Munich, 1992.
54. de Candia, F.; Romano, G.; Baranov, A. O.; Prut, E. V. J Appl Polym Sci 1992, 46, 1799.